Chapter 1

Introduction

> *"Dear Radioactive Ladies and Gentlemen[,]*
> *As the bearer of these lines, to whom I graciously ask you to listen, will explain to you in more detail, beacuse of the 'wrong statistics of N and Li-6 nuclei and the continuous beta spectrum', I have hit upon a desperate remedy to save the 'exchange theorem' of statistics and the law of conservation of energy. ..."*
>
> - W. Pauli, Dec 4, 1930

1.1 β Decay and the Neutrino

In the 1920s, three elementary particles were known: the electron, the proton and the photon. The models of the atomic nuclei were built out of these particles. A nucleus of atomic number **A** and charge **Z** was assumed to be made of **A** positive protons and **A-Z** negative electrons. As such, beta (β) decay was believed to be two-body decay process,

$$N(A, Z) \rightarrow N(A, Z + 1) + e^{-} \tag{1.1}$$

This model suffered from three very severe problems:

1. **Order of magnitude of the energy of electrons measured in β-decay**: The electrons emitted in β-decay process were thought to be present in the nucleus even before the decay. In such cases, their wave function had to be confined in the nuclear size (of the order of 10^{-15} m). And, the uncertainity principle predicts a typical electron momentum and kinetic energy of about 100 MeV. But the observed maximum energies in beta decays were one order of magnitude smaller.

2. **The continuous β-decay energy spectra**: If the β-decay takes place as in Equation 1.1, the electron energy spectra should be a line at the mass difference $m(A, Z) - m(A, Z + 1)$. But experiments showed a continuous spectrum ending at that mass difference [1].

3. **The nuclear statistics**: Between 1928 and 1929, Rasetti measured the Raman rotation spectra of a number of diatomic gases[2], particularly of homonuclear molecules like H_2, N_2 and O_2. The rotational bands he observed showed a sequence of lines of alternate intensity. From the spectra of Rasetti and the explanation of Fermi in his book, it was learned that N_2 nuclei obey Bose statistics [3]. However, N_2 nucleus contained 14 protons and 7 electrons, a total of 21 spin-half particles and its spin should have been half-integral.

In 1930, Wolfgang Pauli postulated a hypothesis[4] stating that a new 'invisible' particle is emitted together with the electron in β-decay, such that the sum of energies of the particle and the electron is constant. This idea explains the conitnuous energy spectrum of β-electrons. Enrico Fermi, in 1933, formulated the theory of β-decay[5] based on Pauli's hypothesis and the new particle was named '*neutrino*' (ν).

Previously, in 1932, J. Chadwick discovered the neutron[6] and its presence in the nucleus together with the protons could solve the problem of the *wrong statistics*. Further, in December 1933, Fermi published his article titled "*Tentativo di una teoria deel'emissione di raggi beta*"[7] and in an extended version, in *Il Nuovo Cimento* where he explained the theory of β-decay of radioactive substances, built on the hypothesis that the electrons emitted by the nuclei do not exist before the decay. Thus, all β-decays were due to the same underlying three-body decay

process

$$n \rightarrow p + e^- + \bar{\nu} \tag{1.2}$$

The first-ever experimental evidence of neutrino took place by observing inverse β-decay reaction in 1956 from the Savannah River reactor plant in South Carolina by F. Reines and C. L. Cowan[8]. Thereafter, the physics community in various corners of the world started conducting underground experiments and a few experiments have been upgraded from time to time to understand this elusive particle. The other two active neutrinos, viz. muon neutrino (ν_μ) and tau neutrino (ν_τ) were directly observed in 1962[9] and 2000[10] respectively.

1.2 Neutrinos in the Standard Model

The discoveries of different fundamental particles (including neutrinos) in the middle of the 20th century necessitated the formulation of a basic theory to understand the properties of these particles and how they interact. The Standard Model (SM) [11, 12] of particle physics, which unifies the electromagnetic, weak, and strong forces, was developed over the course of the second half of the 20th century. Upon experimental verification of quark existence in the middle of the 1970s, the current formulation was finalised. Mathematically, SM is a non-abelian gauge theory based on the symmetry group $U(1)_Y \times SU(2)_L \times SU(3)_c$. Right-handed fermions are SU(2) singlets in this model, while left-handed fermion fields are SU(2) doublets. SM has three generations of leptons and quarks as tabulated in Table 1.1. Every quark has three SU(3) colour charges: red, green and blue. The weak force is carried by the $W^\pm$ and Z^0 bosons, the electromagnetic force is carried by the photon, and the strong force is carried by the gluons. By exchanging

Table 1.1: The structure of quarks and leptons in the SM. 'L' and 'R' stand for left and right-handed particles.

Quarks			**Leptons**		
$\begin{pmatrix} u \\ d \end{pmatrix}_L$	$\begin{pmatrix} c \\ s \end{pmatrix}_L$	$\begin{pmatrix} t \\ b \end{pmatrix}_L$	$\begin{pmatrix} \nu_e \\ e \end{pmatrix}_L$	$\begin{pmatrix} \nu_\mu \\ \mu \end{pmatrix}_L$	$\begin{pmatrix} \nu_\tau \\ \tau \end{pmatrix}_L$
u_R	c_R	t_R	ν_{eR}	$\nu_{\mu R}$	$\nu_{\tau R}$
d_R	s_R	b_R	e_R	μ_R	τ_R

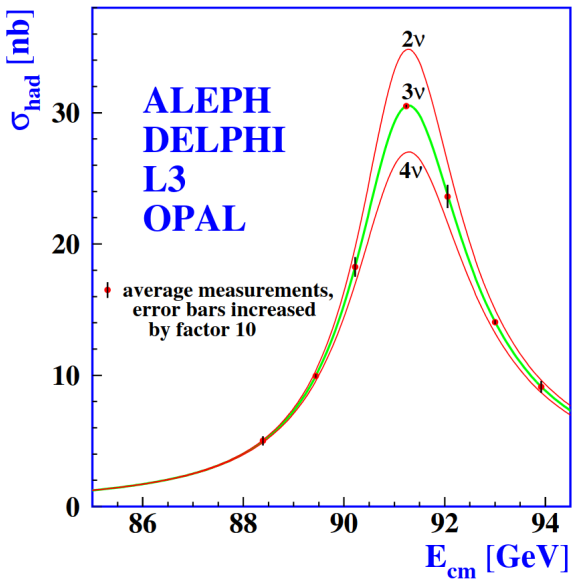

Figure 1-1: Measurements of the hadron production cross-section around the Z^0 resonance. The curves indicate the predicted cross-section for two, three and four neutrino species with SM couplings and negligible mass [13].

$W^{\pm}$ and Z^0 bosons, neutrinos interact weakly with the other leptonic fields in this model. Charge current (CC) interactions are those mediated by the $W^{\pm}$ boson, whereas neutral current (NC) interactions are those mediated by the Z^0 boson.

The number of light neutrino species in SM with the typical electroweak interactions can be counted as follows: The Z^0 boson can decay to the invisible $\nu\bar{\nu}$ pairs according to SM. The difference between Z^0-boson's total decay width and it's visible decay width is known as the invisible decay width. The sum of the Z-boson's partial widths of decay into quarks and charged leptons is referred to as the visible decay width. The ratio of the invisible decay width of Z-boson and the it's decay width to charged leptons (Γ_{inv}/Γ_{ll}) is measured using data from the LEP, and it is found to be 5.943 ± 0.016. ($\Gamma_{\nu\nu}/\Gamma_{ll}$) is the ratio of the partial widths to neutrinos and to charged leptons, and its SM value is 1.99125 ± 0.00083. The number of the light active neutrino species N_ν can be calculated to be 2.9840 ± 0.0082 using this formula ($\Gamma_{inv}/\Gamma_{ll} = N_\nu \Gamma_{\nu\nu}/\Gamma_{ll}$) [13] . This is consistent with the fact that there are only three light active neutrinos known from experiments till date.

Even though SM has a strong track record of success in making predictions that can be verified experimentally and is a mathematically self-consistent model, there

are some limitations. The neutrinos' mass is one of them. Prior to symmetry breaking of the group in SM, the masses of the fermions and gauge bosons are zero. After the spontaneous symmetry breaking, the Higgs mechanism provides masses to the gauge bosons. The masses of the fermions are also determined by the Higgs mechanism. The mass term of the fermions arise from the Yukawa term which is written as: $-y\bar{\psi}_L\psi_R\langle\phi\rangle$, where y is the Yukawa coupling, ψ_L , ψ_R are the left-handed and right-handed fermionic fields respectively and $\langle\phi\rangle$ is the vacuum expectation value (VEV) of the Higgs field. Because there is no suitable right-handed partner, neutrinos cannot have a gauge invariant mass term. Due to the observation of parity violation in weak interactions, right-handed neutrinos are absent in SM. In 1956, Lee and Yang hypothesised that parity is broken in weak interactions, as a solution to the $\tau - \theta$ puzzle[14]. Wu's experiment was the first to observe the parity violation in weak interactions. When the nuclear spins of ^{60}Co were aligned by an external magnetic field, an asymmetry in the direction of the emitted electrons were observed[15]. The decay process under consideration was

$$^{60}Co \rightarrow ^{60} Ni + e^- + \bar{\nu}_e$$

It was discovered that the electron's nuclear spin always acted in opposite direction to its momentum. In other words, the presence of e_L and $\bar{\nu}_R$ alone can account for the observed correlation between the nuclear spin and the electron momentum. The lack of "mirror image" states $\bar{\nu}_L$ and ν_R revealed a blatant parity violation. According to an experimental measurement made by Goldhaber, Grodzins, and Sunyar in 1958, neutrinos are left-handed and antineutrinos are right-handed [16]. Neutrinos are massless in the Standard Model (SM), but the experimentally observed phenomenon known as "neutrino oscillation" suggests that neutrinos have a mass.

1.3 Neutrino Oscillation

The three known neutrino flavour states (ν_e, ν_μ, ν_τ) are expressed as quantum superpositions of three massive states ν_k ($k = 1, 2, 3$) with different masses m_k

with a 3×3 unitary mixing matrix $U_{\alpha k}(\alpha = e, \mu, \tau)$, known as PMNS (Pontecorvo-Maki-Nakagawa-Sakata) matrix U_{PMNS}[17, 18], given by

$$U_{PMNS} = U_{\alpha k} = \begin{bmatrix} U_{e1} & U_{e2} & U_{e3} \\ U_{\mu 1} & U_{\mu 2} & U_{\mu 3} \\ U_{\tau 1} & U_{\tau 2} & U_{\tau 3} \end{bmatrix}$$

The U_{PMNS} matrix can be decomposed as:

$$\begin{bmatrix} \cos\theta_{12} & \sin\theta_{12} & 0 \\ -\sin\theta_{12} & \cos\theta_{12} & 0 \\ 0 & 0 & 1 \end{bmatrix} \begin{bmatrix} \cos\theta_{13} & 0 & \sin\theta_{13}e^{-i\delta_{CP}} \\ 0 & 1 & 0 \\ -\sin\theta_{13}e^{i\delta_{CP}} & 0 & \cos\theta_{13} \end{bmatrix} \begin{bmatrix} 1 & 0 & 0 \\ 0 & \cos\theta_{23} & \sin\theta_{23} \\ 0 & -\sin\theta_{23} & \cos\theta_{23} \end{bmatrix} \cdot M \quad (1.3)$$

and characterized by three non-zero angles $\theta_{kl} \in [0, \frac{\pi}{2}]$ $(k, l = 1, 2, 3$ and $k < l)$ and a charge-parity violating phase $\delta_{CP} \in [0, 2\pi]$. The matrix M has a value of det $M = 1$ for the Dirac neutrinos and $M = diag(1, e^{i\alpha_2}, e^{i\alpha_3})$ for Majorana neutrinos[19]. The mixing angles θ_{kl} are associated with solar, atmospheric and reactor neutrinos given by θ_{12}, θ_{23} and θ_{13} respectively, the mass-squared differences i.e. the mass splitting terms being Δm^2_{21}, Δm^2_{32} and Δm^2_{31} with $\Delta m^2_{kl} = m^2_k - m^2_l$. Thus, the PMNS matrix for Dirac neutrinos can be written as:

$$U_{\text{PMNS}} = \begin{pmatrix} c_{12}c_{13} & s_{12}c_{13} & s_{13}e^{-i\delta_{CP}} \\ -s_{12}c_{23} - c_{12}s_{13}s_{23}e^{i\delta_{CP}} & c_{12}c_{23} - s_{12}s_{13}s_{23}e^{i\delta_{CP}} & c_{13}s_{23} \\ s_{12}s_{23} - c_{12}s_{13}c_{23}e^{i\delta_{CP}} & -c_{12}s_{23} - s_{12}s_{13}c_{23}e^{i\delta_{CP}} & c_{13}c_{23} \end{pmatrix} \quad (1.4)$$

The mass splitting terms can be expressed as:

$$\Delta m^2_{21} = m^2_2 - m^2_1, \quad \Delta m^2_{3n} = m^2_3 - \frac{(m^2_2 + m^2_1)}{2} \quad (1.5)$$

such that, $\Delta m^2_{21} > 0$ and $\Delta m^2_{3n} \equiv \Delta m^2_{31} > 0$ is positive for Normal Mass Ordering (NO) and $\Delta m^2_{3n} \equiv \Delta m^2_{32} < 0$ is negative for Inverted Mass Ordering (IO) for the neutrino mass spectrum. In neutrino oscillations, the diagonal Majorana phase matrix **M** does not have any effect.

Neutrino oscillation is typically measured by comparing the flux of produced α-flavor neutrinos and flux of β-flavor neutrinos observed in a detector placed at

some distance from the production source. The probability for an α-flavor to oscillate into β-flavor, $P_{(\nu_\alpha \to \nu_\beta)}$, depends on three mixing angles $(\theta_{12}, \theta_{13}, \theta_{23})$, CP violation phase $\delta_{\rm CP}$, two mass-squared splittings $(\Delta m^2_{21},\ \Delta m^2_{31})$, its energy E_ν, propagation distance L, and the density of matter passed through by the neutrino ρ, given by

$$P_{(\nu_\alpha \to \nu_\beta)} = f\left(\theta_{12}, \theta_{13}, \theta_{23}, \delta_{CP}; \Delta m^2_{21}, \Delta m^2_{31}; E_\nu, L, \rho\right).$$

It is well-established from the contribution of many neutrino experiments [12] using both the natural neutrino sources (solar and atmospheric neutrinos) and the man-made neutrino sources (reactor and accelerator neutrinos) that the two leptonic mixing angles θ_{12} and θ_{23} are large, θ_{13} is relatively small but non-zero, the mass-squared splitting $|\Delta m^2_{31}|$ is about 30 times larger than Δm^2_{21}. A detailed formulation of neutrino oscillation probabilities has been addressed in Chapter 2.

1.4 Sources of Neutrinos

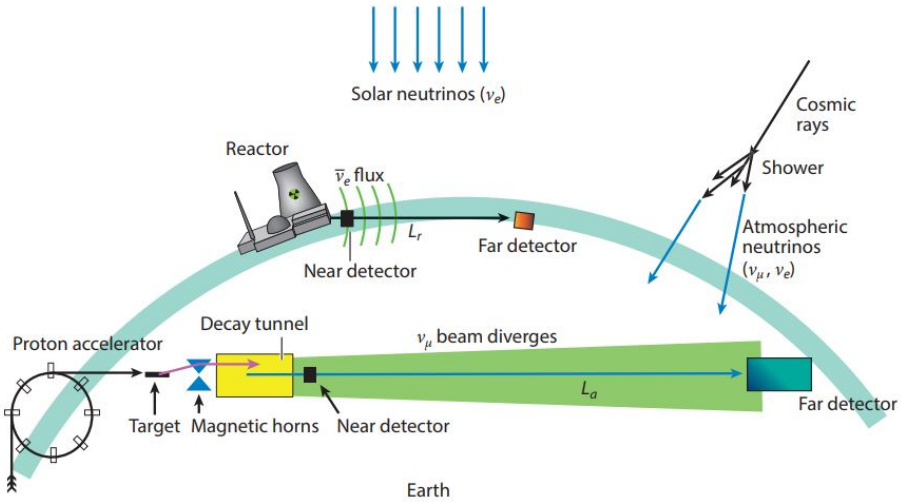

Figure 1-2: Natural and artificial sources of neutrino in a nutshell[20].

Neutrinos are the most aboundant massive particles in the universe. They are produced in the stars, Earth's atmosphere, supernovae and active galactic nuclei. The man-made sources include neutrino production in nuclear fission in

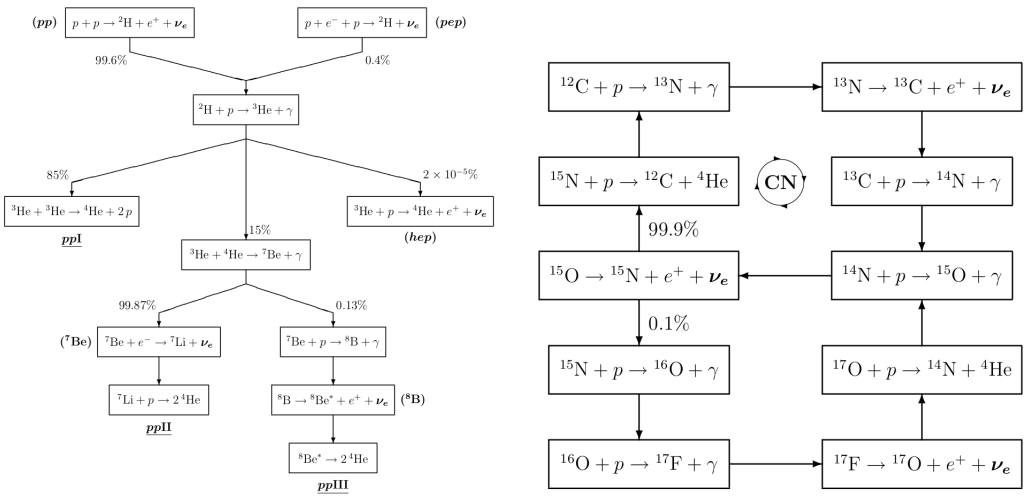

Figure 1-3: The pp (CNO) chain of the solar thermonuclear reaction in shown in the left (right) figure. The produced neutrinos are depicted in bold fonts [21] .

reactors and through pion decay in accelerators. Neutrinos are also produced in the core of the sun through nuclear fusion reactions.

1.4.1 Natural Sources

1.4.1.1 Solar Neutrinos

The major contribution comes from proton-proton (pp) and CNO reactions. More than 99% of the solar neutrinos are produced in the pp process. Neutrino are also produced during production of ^7Li and ^8B nuclei. The solar neutrinos are electron neutrinos in nature. The deuteron with another proton produces a Helium (^3He) nuclues and gamma ray which further results in production of ^4He isotope. Both the Helium isotopes now fuse to form Beryllium (^7Be) and a gamma ray. The ^7Be, then, undergoes electron/proton capture to produce $^7Li/^8B$ and electron-neutrino. Detection of electron neutrinos are also reported from depth of the solar core through carbon-nitrogen-oxygen (CNO) cycle.

The processes involved in the pp and CNO reactions are given in Figure 1-3. Solar neutrinos were first detected in 1968 in the Homestake experiment[22], confirmed by Kamiokande. The low-energy neutrinos produced in the pp-reaction were measured by the gallium experiments.

The Homestake experiment is a radiochemical experiment which detect solar neutrinos using Inverse beta decay (IBD) reaction[23, 24], given by

$$\nu_e + {}^{37}Cl \rightarrow {}^{37}Ar + e^-$$

with a neutrino threshold energy of 0.814 MeV, and thus, can detect only intermediate and high-energy neutrinos. The experiment is mainly sensitive to the high-energy ^8B neutrinos. The solar neutrino flux recorded by the experiment was less than 3 Solar Neutrino Units (SNU)[1], which about 1/3 of that predicted by the Standard Solar Model (SSM)[25]. The gallium experiments like GALLEX [26–30], GNO [31, 32] and SAGE [33–37] detected solar neutrinos using gallium (^{71}Ga) as the detection target, with low neutrino energy threshold of 233 keV[38]. Thus, these experiments are sensitive to all sources of solar neutrinos. The solar neutrino flux measured by these experiments are about 1/2 of that predicted by the SSM. The Kamiokande [39, 40] (Super-Kamiokande [41]) experiment, with a water Cherenkov dectector, is sensitive to ^8B solar neutrinos with the neutrino energy threshold range of 6.7-9.0 (4.7-6.2) MeV. The experiment measured the solar neutrino flux via the elastic scattering (ES) reaction, and the average flux of ^8B ν_e obtained is about half the SSM flux.

In the late 20th century, another breakthrough experiment, SNO [42] provided measurements on the high energy part of the solar neutrino flux. SNO detects solar neutrino through three reactions on the deuterium target: the charged current (CC), the Neutral current (NC) and ES. Due to high backgrounds at low energies, the corresponding neutrino energy threshold are 6.9, 2.224 and 5.7 MeV respectively, all of the reactions being sensitive to ^8B solar neutrinos. The results confirmed the solar ν_e deficits [43], observed by the previous experiments. The NC measurement of the total flux observed that two ν_e out of three converts into ν_μ or ν_τ on their way from the center of the Sun to the Earth [44]. Thus, SNO experiment is significant for it proved that the solar neutrino problem (SNP) is due to neutrino flavour transitions.

[1] 1SNU$\equiv 10^{-36}$ events/atom/s

1.4.1.2 Atmospheric Neutrinos

Atmospheric neutrinos are typically produced around 15 kilometers above Earth's surface. They form when a cosmic ray, high energetic particles (mostly protons) from space interact with the Earth's atmosphere. When they strike an atomic nucleus in our atmosphere, there is a cascade of particles. Short-lived particles called mesons form, most of them pions (and a few kaons). These are unstable particles made of two quarks, and they rapidly decay into muons and muon antineutrinos (or antimuons and muon neutrinos). A muon, being unstable, also undergoes decay into an electron, electron antineutrino, and muon neutrino. About two- thirds of atmospheric neutrinos are muon neutrinos and antineutrinos, and the remainder are electron neutrinos and antineutrinos. The reactions involved in the process are-

$$\begin{aligned} p + X(hadron) \rightarrow \pi^{\pm}(K^{\pm}) \rightarrow \mu^{\pm} + \nu_{\mu}(\bar{\nu_{\mu}}) \text{ (primary/dominant decay)} \\ \mu^{\pm} \rightarrow e^{\pm} + \nu_e(\bar{\nu_e}) + \bar{\nu_{\mu}}(\nu_{\mu}) \text{ (secondary decay)} \\ K^{\pm} \rightarrow e^{\pm} + \nu_e(\bar{\nu_e}) + \pi^0 \end{aligned}$$

Atmospheric neutrinos were first detected in the mines of Kolar Gold Fields [45] of India and at the same time in a gold mine of South Africa [46]. From the above decay chain, the expected number of muon neutrinos (N_{μ}) are about twice that of electron neutrinos (N_e).

$$\text{i.e.} \quad \frac{N_{\mu} + N_{\bar{\mu}}}{N_e + N_{\bar{e}}} \sim 2 \tag{1.6}$$

However, experiments like Kamiokande [47], IMB [48, 49] and Sudan2 [50] reported the ratio of observed N_{μ}/N_e to that of Monte-Carlo simulation, to be significantly less than one. This is known as the "Atmospheric Neutrino Anomaly". The Super-Kamiokande (SK) [51] detector started the operation in 1996 and concluded that the anomaly is due to $\nu_{\mu} \rightarrow \nu_e$ or $\nu_{\mu} \rightarrow \nu_{\tau}$ flavour oscillations. Apart from that, the oscillatory behaviour can be tested by observing neutrinos with different incoming directions that have travelled different distances to the detector. This

is parameterised by the zenith angle[2]. Atmospheric neutrino flux peaks at zenith angle $\sim 90^\circ$ (near the horizon), due to larger length of the atmosphere in that direction. For downward moving neutrinos, different zenith angles have path length of range $\sim 10 - 30km$, whereas, the upward moving neutrinos suffers significant oscillatory behaviors due to its larger path length of $\sim 10^4 km$ for different zenith angles. Neutrinos are also produced in distant astrophysical sources [52] such as supernovae [53, 54], active galactic nuclei (AGN) [55] and gamma ray burst (GRB) [56].

Neutrino oscillation experiments are classified on the basis of the sources of the neutrinos and the measurements of appearance and disappearance channels. Their classification also depends on the average value of the ratio $\frac{L}{E}$ for an experiment, which determines the sensitivity to the mass-squared differences Δm^2_{ij} $(i = 1, 2, 3)$. It is to be noted that,

$$UU^\dagger = 1 \text{ gives } \sum_{k=1}^{3} U_{\alpha k} U^\dagger_{\beta k} = \delta_{\alpha\beta} \tag{1.7}$$

which implies $P_{\nu_\alpha \to \nu_\beta}(L = 0, E) = \delta_{\alpha\beta}$. For $L > 0$, the amplitude of the oscillations is specified by the elements of the lepton mixing matrix U and the phases allow us to obtain information on the values of mass-squared differences Δm^2_{ij}. The oscillation length L^{osc}_{ij} is the distance at which the phase generated by Δm^2_{ij} becomes maximum, equal to 2π.

$$L^{osc}_{ij} = \frac{4\pi E}{\Delta m^2_{ij}} \tag{1.8}$$

Considering the above fact, different experiments are designed in order to be sensitive to Δm^2_{ij}, for which

$$\frac{4\pi E}{\Delta m^2_{ij} L} = 2\pi \Leftrightarrow \frac{\Delta m^2_{ij} L}{2E} \sim 1 \Leftrightarrow \Delta m^2_{ij} \propto \frac{E}{L} \tag{1.9}$$

The classification of neutrino oscillation experiments with their source-detector distance (L), energy (E) and sensitivity to Δm^2_{ij} [which is given by E/L, E in MeV

[2]Zenith angle is the angle between the neutrino direction and the vertical.

Table 1.2: Classification of neutrino oscillation experiments with their source-detector distance (L), energy (E) and sensitivity to Δm^2_{ij}.

Type of Experiments	L	E	Δm^2_{ij} sensitivity
Reactor SBL	∼10m	∼1 MeV	∼0.1 eV^2
Accelerator SBL (Pion DIF)	∼1km	≥1 GeV	≥1 eV^2
Accelerator SBL (Muon DAR)	∼10m	∼10 MeV	∼1 eV^2
Accelerator SBL (Beam Dump)	∼1km	∼100 GeV	$\sim 10^2$ eV^2
Reactor LBL	∼1km	∼1 MeV	$\sim 10^{-3}$ eV^2
Accelerator LBL	$\sim 10^3$km	≥1 GeV	$\geq 10^{-3}$ eV^2
Reactor VLB	$\sim 10^2$km	∼1 MeV	$\sim 10^{-3}$ eV^2
Accelerator VLB	$\sim 10^4$km	≥1 GeV	$\geq 10^{-4}$ eV^2

(GeV) and L in m (km) for reactor (acceleartor-based) neutrino experiments] is listed in Table 1.2.

1.4.2 Terrestrial Neutrino Sources

Terrestrial neutrino oscillation experiments (TNE) use neutrinos produced in reactors and accelerators. The sensitivity *i.e. the capability of an experiment to measure the oscillation parameters* depends importantly on source-detector distance, the neutrino energy, the power of the source, the detection cross-section and the backgrounds. In TNEs, one can control the values of these factors.

1.4.2.1 Reactor-based neutrino

When neutrinos have enough energy to produce charged particles like the electron (0.511 MeV), muon (105.7 MeV), or tau (1776.8 MeV), they can be detected through charged current interactions. Only reactions that produce positrons are feasible because the reactor neutrino energy is low. The inverse neutron decay process allows for the detection of reactor electron antineutrinos. This reaction liberates a total vivisble energy $E_e + m_e$, where E_e is the energy of the positron, which annihilates with the surrounding electron. This energy can be seen in scintillation detectors. The antineutrinos can be distinguished from the background by the coincidence of the prompt signal with the delayed signal produced by the nuclear capture of the neutron. Neglecting the small recoil energy

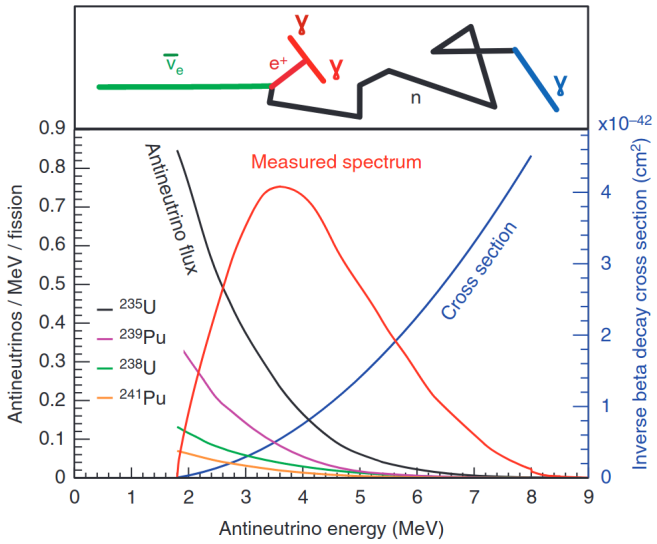

Figure 1-4: An observable electron anti-neutrino ($\bar{\nu}_e$) spectrum in reactor neutrino experiment [57].

of the neutron, the neutrino and positron energies are related by

$$E_\nu = E_e + T_n + m_n - m_p \simeq E_e + 1.293MeV \tag{1.10}$$

where T_n is the negligibly small recoil kinetic energy of the neutron. Thus, the neutrino energy threshold is given by

$$E_\nu^{th} = m_n + m_e - m_p \simeq 1.804eV \tag{1.11}$$

The response of a detector to a reactor electron anti-neutrino ($\bar{\nu}_e$) flux is illustrated in Fig. 1-4 which is proportional to the product of the

- antineutrino fluxes from each isotope, and
- the detection cross-section.

R-SBL experiments have source-detector distances between 10-100m. ILL [58], Gosgen [59], Rovno [60], Krasnoyarsk [61], Bugey [62] and Savannah River [63] were operative in the 1970s, but none of them observed a $\bar{\nu}_e$ disappearance. Their L values were sufficient to reach the sensitivity to the small values of Δm^2_{ij}. Long baseline (LBL) reactor-based neutrino osillation experiments with baselines of

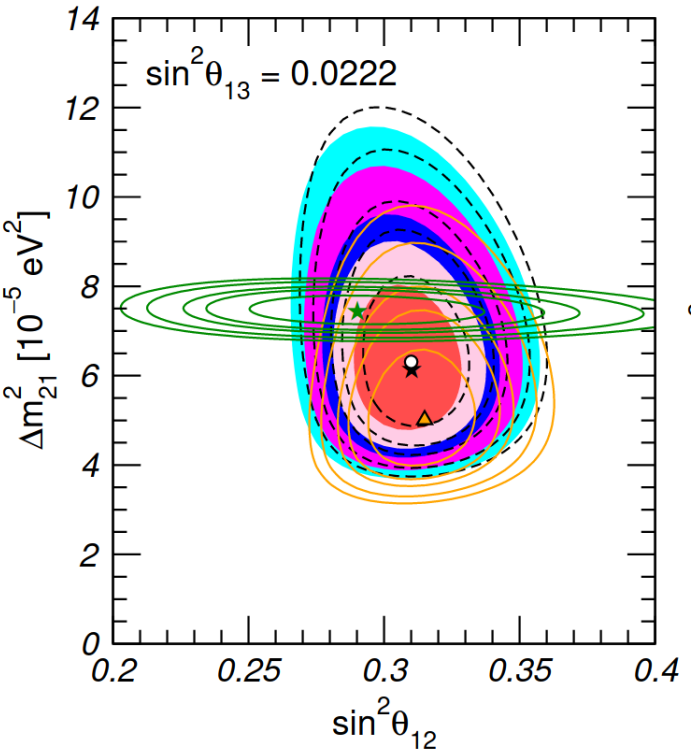

Figure 1-5: Allowed regions of $\sin^2\theta_{12} - \Delta m^2_{21}$ for fixed $\theta_{13} = 8.6°$ for solar and KamLAND data, with and without Super Kamiokande results. The updated allowed regions are showed at 1σ, 90%, 2σ, 99% and 3σ C.L for 2 d.o.f.. The analysis for KamLAND is given by solid green contours with best fit marked by a green star [75].

the order of 1 km have the sensitivity of Δm^2 of about $10^{-3}eV^2$, corresponding to atmospheric mass-squared difference. Chooz [64–66] and Palo Verde [67–69] are the notable experiments that were carried out in the 1990s. Although, these experiments were important to understand the reactor neutrino flux and spectrum, yet unable to observe the oscillation of $\bar{\nu}_e$ disappearance. However, they obtained an upper limit of $\sin^2\theta_{13} < 0.10$ at 90% C.L. [65].

In the next-generation reactor experiments, Daya-Bay[70, 71], RENO [72] and Double Chooz [73, 74], our knowledge of the value of the element U_{e3} of the lepton mixing matrix in the case of three-neutrino mixing was further clarified. They solved the puzzle of the value of the mixing angle, θ_{13}, which finally turned out to be non-zero. The present best-fit value of the mixing angle from the reactor experiments is $\sim 8.6°$, dominated by Daya Bay result [75, 76].

The KamLAND experiment [77] has been designed to detect electron

antineutrinos produced by 53 nuclear power reactors in Japan, with a small contribution from reactors in South Korea ($\sim$ 2%), at distances varying from 80 km to 800 km. About 80% of the detected neutrinos come from reactors at distances between 140 km and 215 km, with an average distance of about 180 km. The large source–detector distance allowed the KamLAND experiment to measure the $\bar{\nu}_e$ disappearance due to the small solar Δm^2_{21}. The ratio of measured to expected $\bar{\nu}_e$ events in KamLAND from March 2002 to January 2004 [78] is

$$R = 0.658 \pm 0.044 \pm 0.047$$

which deviates from unity by about 5σ. It showed that the earlier solar neutrino measurements were indeed caused by oscillations. It also measures the most accurate value of the mass-squared difference Δm^2_{21}. The present allowed regions of $\sin^2\theta_{12} - \Delta m^2_{21}$ plane obtained with a combined fit of KamLAND and solar data is presented in Figure 1-5. The present best-fit values [75] of the solar mixing parameters are:

$$\Delta m^2_{21} = 7.42 \times 10^{-5} eV^2, \quad \sin^2\theta_{12} = 0.304 \text{ (for both the mass hierarchies)}$$

Another type of experiments are reactor-based medium baselines (MBLs) like JUNO which due to its unique baseline of 52.5 km is sensitive to both the solar and atmospheric mass-squared differences.

1.4.2.2 Accelerator-based neutrino

In accelerator neutrino oscillation experiments, neutrinos and anti-neutrinos are produced when high energetic proton beam collide a fixed hadronic target. The proton beam is accelerated by a set of linear and cycling synchotrons to achieve a higher energy before hitting the target. The proton collision with the fixed target mainly produces pions ($\pi^{\pm}$) and kaons ($K^{\pm}$). This meson beam is aligned (*defocused, to be accurate*), into a decay pipe, where they decay primarily into charged muons and muon neutrinos or muon anti-neutrinos depending on the parent mesons. The charged muons can further undergo secondary decay into

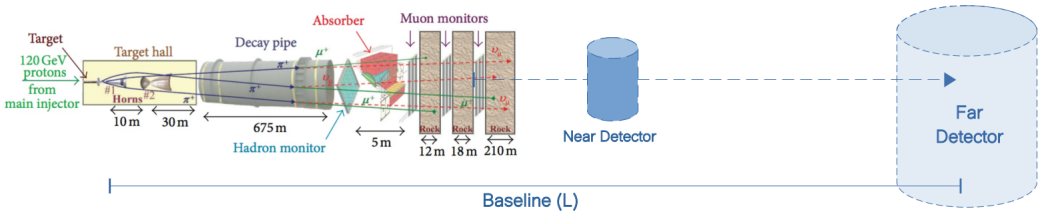

Figure 1-6: Process of neutrino production, propagation and detection in accelerator neutrino oscillation experiments. The left portion of the image is the NuMI beamline [79] which are employed in the MINOS [80], MINOS+ [81] and NOνA [82] experiments.

electron neutrino and anti-neutrino, resulting in the contamination of the highly intense muon neutrino (anti-neutrino) beam. The following processes take place:

$$\pi^{\pm}(K^{\pm}) \longrightarrow \mu^{\pm} + \nu_{\mu}(\bar{\nu}_{\mu}) \quad \text{(most dominant)}$$

Secondary decay may take place resulting in ν_e, given by

$$\mu^{\pm} \longrightarrow e^{\pm} + \nu_e(\bar{\nu}_e) + \bar{\nu}_{\mu}(\nu_{\mu})$$

$$K^{\pm} \longrightarrow e^{\pm} + \nu_e(\bar{\nu}_e) + \pi^0$$

The charged leptons are stopped by the absorber and, the neutrinos and anti-neutrinos travel to the far detector (FD) traversing a distance L(in km) beneath the earth's surface where the oscillation analysis is performed. In present days, near detectors (ND) are placed close to the source of production to reduce the uncertainity in flux and cross-section information. ND monitors the un-oscillated ν_{μ} and $\bar{\nu}_{\mu}$ fluxes from the production site. Figure 1-6 illustrates the production, propagation and detection of the neutrino beam as described above.

Accelerator experiments can be classified according to their source-detector baselines (L) in Table 1.2 and the method of production of the neutrino beam are pion decay in flight (DIF), muon decay at rest (DAR) and beam dump.

1. **Pion Decay in Flight (DIF)**: Neutrino beam is produced by the decay of mesons, most dominantly pions, created by a proton beam after hitting a target. The pions and kaons are aligned in a decay tunnel for decay

of mesons to neutrinos and antineutrinos. The neutrino thus produced is primarily composed of ν_μ or $\bar{\nu}_\mu$. The typical energy of the neutrinos vary from sub-GeV to few GeV depending on the energy of the initial proton beam.

They can also be further sub-divided based on the neutrino beams generated by pion decay in flight, in three categories:

a. *Wide band beam:* These are experiments having a high-intensity neutrino beam with a wide energy spectrum which can span one or two orders of magnitude. This type of beam is convenient for investigating new oscillation signals in a wide range of values of Δm^2_{ij}.

b. *Narrow band Beam:* The neutrino beams of these experiments have a narrow energy spectrum, which is obtained by selecting the momenta of the parent pion and kaons. The resulting intensity of the neutrino flux of a narrow-band beam is reduced comparing with a wide-band beam obtained from the same proton beam. Narrow-band beams are convenient for precise measurements of Δm^2_{ij}.

c. *Off-Axis Beam:* These are experiments which use a high-intensity wide-band beam with the detector shifted by a small angle from the axis of the beam, where the neutrino energy is almost monochromatic. The off-axis principle is a new concept, which is exploited by LBL experiments T2K and NOνA. The neutrino energy as a function of the parent pion energy (E_π) and off-axis angle (θ), for pions, is given by:

$$E_\nu = \frac{\left[1 - \frac{m_\mu^2}{m_\pi^2}\right] E_\pi}{1 + \gamma^2 \theta^2}, \tag{1.12}$$

And the expression for the neutrino flux as a function of the angle is,

$$\phi_\nu(\theta) \propto \left(\frac{2\gamma}{1 + \gamma^2\theta^2}\right)^2, \tag{1.13}$$

to the lowest order of θ, where $\gamma = \frac{E_\pi}{m_\pi}$, is the Lorentz factor. For $\theta = 0$, the neutrino energy linearly varies with pion energy, whereas it

tails off for $\theta > 0$. To obtain a narrow band beam, one can look for a non-zero off-axis angle and baselines at the ν_e-appearance oscillation maximum. For NOνA, $\theta = 14.6mrad$ at a baseline of 810 km results in the neutrino flux peak at $\sim 2GeV$ (Figure 1-7). Similar Off-axis technique is utilized by the T2K experiment with $L = 295km$ with $\theta = 2.5°$ to obtain a peak in neutrino flux at $0.6GeV$.

2. **Muon Decat At Rest (DAR)**: A beam of low-energetic muon antineutrinos are produced from the decay of the μ^+ produced in the pion decay (the π^- are mostly absorbed by nuclei) and stopped in the target. The process is

$$\mu^+ \rightarrow e^+ + \nu_e + \bar{\nu}_\mu$$

$$\pi^+ \rightarrow \mu^+ + \nu_\mu$$

The antineutrinos have energies of the order of several tens of MeV.

3. **Beam Dump**: In this method, a proton beam of the order of some hundreds of GeV, hit a thick target, called the beam dump, where the proton-nucleon interactions generate heavy hadrons. The charmed heavy hadrons decay promptly with practically equal branching ratios into electrons and muons, emitting equal fluxes of electron and muon neutrinos with energies of the order of 10^2 GeV. A detector at a distance of the order of 1 km can measure the ratio of the electron and muon neutrino fluxes, whose deviations from unity would signal the presence of oscillations [21].

SBL accelerator experiments like CHARM [84], CDHSW [85], CCFR [86], BEBC [87], LSND [88], NOMAD [89], KARMEN[90], CHORUS [91] among others have been carried out to explore the diffrent flavor transition channels. All other experiments except LSND failed to find any indication of neutrino oscillations [92, 93].

K2K is the first generation LBL accelerator-based neutrino oscillation experiment based in Japan, with a distance of 250 km from the source in the KEK laboratory to the Super-Kamiokande detector in the Kamioka mine [94–97]. The neutrino beam is a pulsed wide-band beam with a mean energy of 1.3 GeV. It is an almost

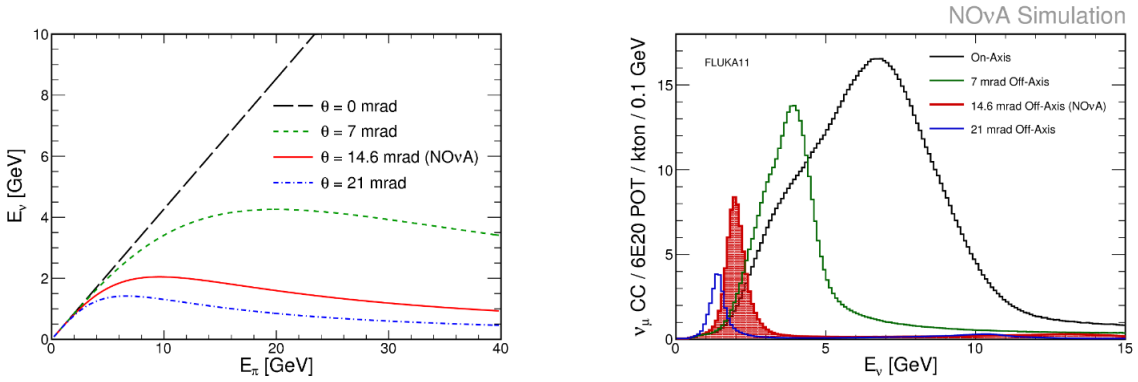

Figure 1-7: Neutrino energy as a function of the parent π-energy for different off-axis angles *(left)* and the overall predicted flux per given exposure *(right)*. The figure is a description of the NOνA experiment [83].

pure ν_μ beam ($\sim 98\%\nu_\mu + \sim 1\%\bar{\nu}_\mu + \sim 1\%\nu_e$). The protons are focused on an aluminum target and the produced positive pions are focused towards a decay tunnel 200 m long, where they decay into antimuons and muon neutrinos. At the end of the decay tunnel, there is an iron and concrete beam dump which stops all charged particles, except muons with energy greater than 5.5 GeV. After the beam dump, there is a muon monitor and after about 70 m of earth which eliminates all particles except neutrinos, there is a near neutrino detector system which is used to calibrate the neutrino beam (about 300 m from the production target). The near detector system consists of two detector sets: a 1 kton water Cherenkov detector and a fine-grained detector system. The water Cherenkov detector uses the same technology and analysis algorithms as the Super-Kamiokande far detector. Another notable accelerator-based LBL experiments include OPERA [98], ICARUS [99], MINOS and MINOS+ (based is the USA, which concluded their data taking in late 2019). Ongoing experiments include the second generation accelerator LBL experiments of Japan and the USA, T2K [100] and NOνA [101] respectively which form the basis of the thesis, are discussed in greater details in the upcoming chapters.

The sources of neutrinos, their detection techniques, description of relevant neutrino experiments and their results are explored in our paper [102] and the literature cited within.

Neutrino Interactions

The neutrino energy accessible to A-LBL neutrinos makes them sensitive to different interaction types as represented by the Feynman diagram in Figure 1-8. The neutrino and anti-neutrino inclusive cross-sections at the intermediate energy range, appropriate for A-LBL, vary from 0.2 to 20 GeV. At these intermediate energies, several distinct neutrino scattering mechanisms start to play a role, as shown in Figure 1-9. They are:

- Quasi-Elastic (QE) scattering,
- Resonant Delta Production (RES),
- Deep Inelastic Scattering (DIS), and
- Meson Exchange Current (MEC).

Quasi-Elastic (QE) scattering: For neutrino energies less than $\sim 2GeV$, neutrino-hadron interactions are predominantly quasi-elastic (QE). They provide large source of signal events in many neutrino oscillation experiments operating in this energy range. In this process, the neutrino scatters off a single nucleon within the nucleus instead of its constituent parton. The target neutron in the detector is converted to a proton when a neutrino is involved, and vise-versa for a

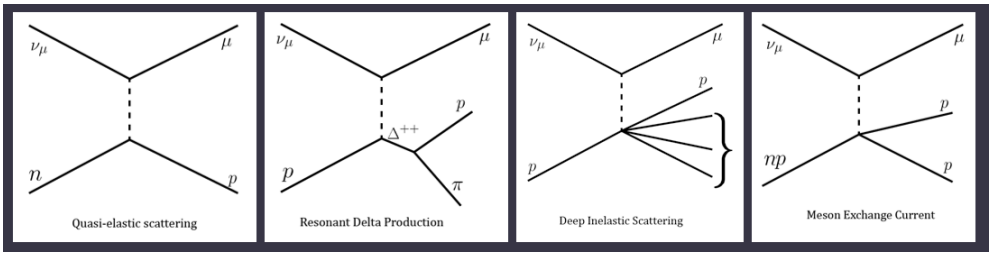

Figure 1-8: Feynman diagrams for different types of neutrinos interactions at the detector. The image is taken from https://www.phys.ksu.edu/reu/2018/song.html.

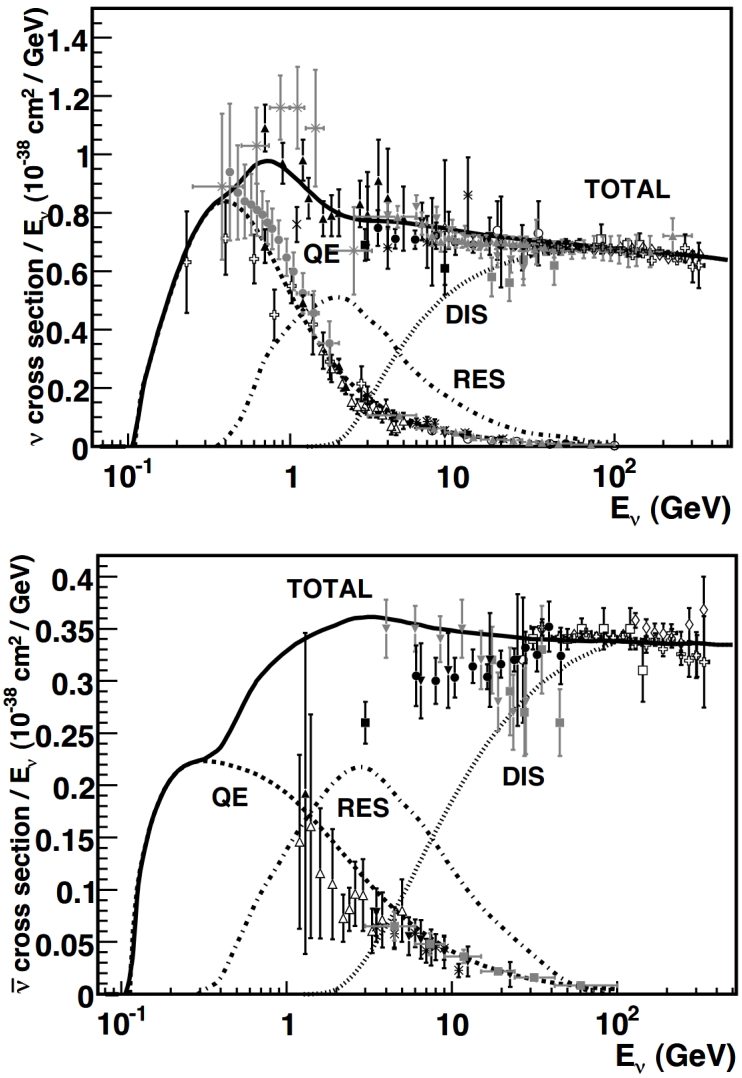

Figure 1-9: The neutrino and antineutrino per nucleon CC cross sections (for an isoscalar target) divided by neutrino energy as a function of energy [103].

antineutrino.

$$\nu_\mu + n \rightarrow \mu^- + p \tag{1.14}$$

$$\bar{\nu}_\mu + p \rightarrow \mu^+ + n \tag{1.15}$$

The overall $Q^2 (= q^2)$ for this interaction is relatively low and QE events are generally characterized by clean lepton signatures travelling relatively in line with the beam direction and a small hadronic component which usually involves a single proton track for the neutrino case.

Resonant Delta Production (RES): These interactions produce baryon resonances in the final state (Δ) which decay into pions and protons. If a π^0 is produced that usually decays via $\pi^0 \rightarrow \gamma\gamma$. Sometimes a single γ can be produced by the Δ decay as well ($\Delta^+ \rightarrow p\gamma$). These can exhibit a variety of signatures but usually involve either charged pion tracks which can hard-scatter in the detector and produce kinks or a pair of electromagnetic shower cascades coming from π^0 decay. Sometimes multiple proton tracks can be seen as well.

Deep Inelastic Scattering (DIS): These are in general messy interactions at a very high Q^2 where the relevant initial state particles involved are the quark soup within each nucleon. The event signature is a large hadronic component due to the resulting hadronization of the final state quarks. Here the lepton signatures aren't very clean, being relatively small and travelling at a large angle with respect to the beam.

Meson Exchange Current (MEC): These are interactions at a slightly higher Q^2 where the neutrino scatters off a correlated nucleon pair instead of a single nucleus. The nucleon pair is predominantly a np pair which produces two protons (neutrons) in the final state for neutrinos (anti-neutrinos).

1.5 Knowns and Unknowns in Neutrino Physics

In the standard 3ν framework, there are six parameters that govern neutrino oscillations: θ_{12}, θ_{13}, θ_{23}, δ_{CP}, Δm^2_{21} and $\Delta m^2_{31(2)}$. Global fit 1[75] and global fit 2[76] are the updated global analysis of the neutrino experiments' datasets and the previous results are available in Ref. [104, 105] respectively. Global fit 1 is also known as NuFit 5.0 and the previous corresponding is called NuFit 4.1. Global fit 1 & 2 include the updated results from Super-Kamiokande, IceCube DeepCore, SNO, short baseline reactor experiments Daya Bay and RENO, long baseline (LBL) accelerator-based neutrino experiments T2K and NOνA upto July 2020 when the Neutrino 2020 conference took place. In Global Fit 1, the authors

Table 1.3: The neutrino oscillation parameters, according to two different global fits- Global Fit 1[75] & Global Fit 2[76].

Global Fit 1	Parameters[a]	Mass Ordering	Best Fit	3σ
	$\Delta m^2_{21}(\times 10^{-5} eV^2)$	NH,IH	7.42	6.82-8.04
	$\theta_{12}(^o)$	NH	33.44	31.27-35.86
		IH	33.45	31.27-35.87
	$\lvert\Delta m^2_{3n}\rvert(\times 10^{-3} eV^2)$	NH	2.517	2.435-2.598
		IH	2.498	2.581-2.414
	$\theta_{23}(^o)$	NH	49.2	40.1-51.7
		IH	49.3	40.3-51.8
	$\theta_{13}(^o)$	NH	8.57	8.20-8.93
		IH	8.60	8.24-8.96
	$\sigma(^o)$	NH	197	120-369
		IH	282	193-352
Global Fit 2	$\Delta m^2_{21}(\times 10^{-5} eV^2)$	NH,IH	7.50	6.94–8.14
	$\theta_{12}(^o)$	NH,IH	34.3	31.4–37.4
	$\lvert\Delta m^2_{3n}\rvert(\times 10^{-3} eV^2)$	NH	2.55	2.47–2.63
		IH	2.45	2.37–2.53
	$\theta_{23}(^o)$	NH	49.26	41.20–51.33
		IH	49.46	41.16–51.25
	$\theta_{13}(^o)$	NH	8.53	8.13–8.92
		IH	8.58	8.17–8.96
	$\sigma(^o)$	NH	194	128–359
		IH	284	200–353

[a] $\Delta m^2_{3n} \equiv \Delta m^2_{31} > 0$, for Normal Hierarchy, Δm^2_{31} being the reactor mass squared difference. $\Delta m^2_{3n} \equiv \Delta m^2_{32} < 0$, for Inverted Hierarchy, Δm^2_{32} being the atmospheric mass squared difference.

assume that the Wilk's theorem holds to convert $\Delta\chi^2$ values into confidence levels and equivalent numbers of Gaussian standard deviations (σ). In Global Fit 2, the authors have considered both Bayesian and frequentist method for oscillation data analysis to arrive at their results.

The global fits give more accurate measurements of oscillation parameters of θ_{12}, θ_{13}, Δm^2_{21} and $|\Delta m^2_{31,32}|$. The sign of $\Delta m^2_{31,32}$ referred as mass hierarchy of the three mass-eigenstates, the resolving of the octant degeneracy of mixing angle θ_{23} and determination of δ_{CP} have been studied extensively in the two global fits. Presently, the 3σ relative precision[3], marginalised over both hierarchies, for the oscillation parameters stands at 4% for θ_{12}, 9% for θ_{13}, 25% for θ_{23}, 16%

[3]Relative precision is defined as $\frac{2(x_1-x_2)}{(x_1+x_2)}$, where x_1 is the upper and x_2 is the lower bound in Table 1.3.

for Δm^2_{21} and 6.5% for $|\Delta m^2_{31,32}|$. The solar mixing angle is well measured by solar experiment while the corresponding mass-squared difference Δm^2_{21} is better constrained by KamLAND. The recent evidence of neutrino flux from CNO fusion chain by Borexino is not included in these analyses. In these updated global fits, the disagreement between solar and KamLAND data has decreased significantly after the inclusion of the updated Super Kamiokande solar neutrino results. The short baseline reactor-based experiments Daya Bay and RENO are sensitive to θ_{13} and $|\Delta m^2_{31,32}|$. The upcoming reactor-based medium baseline experiment JUNO promises to measure the solar parameters apart from θ_{13} and Δm^2_{31} with a better precision. NOνA recently showed evidence of appearance of anti-neutrino with greater thac 4σ C.L. T2K alone excludes the CP conserving values of δ_{CP} at almost 3σ C.L. The best fit value of δ_{CP} for T2K lies near $3\pi/2$ for NH, whereas for NOνA, it is 0.82π- close to CP conversing value π. This tension has to be resolved and a joint-collaboration of T2K and NOνA colleagues has started. However, for inverted hierarchy, the best fit of δ_{CP} is close to $3\pi/2$. T2K has better presion for θ_{13} measurement than NOνA but it is not competitive to that of reactor-based short baseline experiments.

There are many open questions in neutrino physics and we divide them into two categories:
(1) Questions within standard 3ν oscillation framework, and
(2) beyond standard 3ν neutrino oscillation framework.
A few of them are described below.

1.5.1 Questions within standard 3ν oscillation framework

1.5.1.1 Neutrino Mass Hierarchy

The solar experiments confirmed that $\Delta m^2_{21} > 0$ i.e. $m_2 > m_1$, but the sign of Δm^2_{31} is still unknown. Thus, we are left with two possibilities for the mass eigenvalues. We refer them as the mass hierarchies (MH) of the three active neutrinos: (A) Normal Ordering, $m_3 > m_2 > m_1$, and (B) Inverted Ordering,

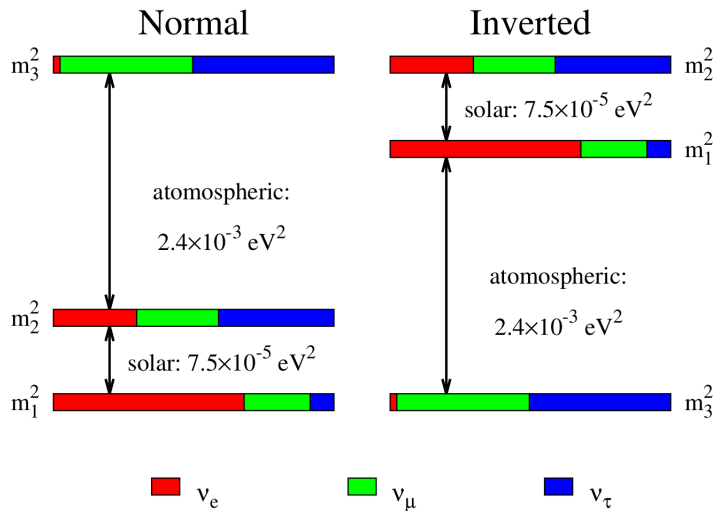

Figure 1-10: Illustration of normal and inverted neutrino mass hierarchies.

$m_2 > m_1 > m_3$. The sign of Δm^2_{31} is of fundamental importance because it has many implications in particle physics and astrophysics. The behavior of neutrino oscillations in atmospheric and long baseline experiments are sensitive to Δm^2_{31} [106]. The supernova neutrino oscillations are also affected for a similar reason [107]. The interference effects of two atmospheric mass-squared differences in reactor neutrino vacuum oscillations is also sensitive to it [108]. Moreover, preference to IO may help the seesaw and leptogenesis [109] mechanisms work well to interpret the tiny neutrino mass and explain the baryon asymmetry of the Universe (BAU) [110, 111]. If the hierarchy is inverted, it also provides a chance to observe neutrinoless double beta decay $0\nu\beta\beta$, and thus the Majorana nature of neutrino [112].

1.5.1.2 Leptonic CP Violation

The CP transformation combines charge conjugation C with parity P . Under C transformation, particles and antiparticles are interchanged, and the handedness of space is reversed under P transformation, $\vec{x} \rightarrow -\vec{x}$. For instance, CP can change a left-handed electron e^-_L into a right-handed positron, e^+_R. The laws of nature would apply to both matter and antimatter if CP were an exact symmetry. Since most phenomena exhibit C and P symmetry, they are also CP symmetric. These symmetries are respected by the gravitational, electromagnetic, and strong

interactions. On the other hand, the weak interactions most severely violate C and P. The charged W bosons, for instance, couple to left-handed electrons, e_L^-, and to their CP conjugate right-handed positrons, e_R^+, but not to their P conjugate right-handed electrons or their C conjugate left-handed positrons. Although weak interactions separately violate C and P, CP is still preserved in most weak interaction processes. However, the CP symmetry can be broken in some extremely rare processes, as seen in neutral K decays in 1964 [113] and later confirmed in B (2001) and D (2019) decays [12].

It is crucial to know whether or not the CP symmetry in the leptonic sector is violated because it will explain the observed baryon asymmetry of the universe (BAU) via leptogenesis. Under CPT invariance, CP violating asymmetries is measured by appearance channels, particularly in A-LBL, given by $A_{CP}^{\alpha\beta} = P(\nu_\alpha \to \nu_\beta) - P(\bar{\nu}_\alpha \to \bar{\nu}_\beta)$, where $\alpha, \beta = e, \mu, \tau$. $A_{CP}^{\alpha\beta}$ depends on all the six oscillation parameters. Given that θ_{12} and Δm^2_{21} are well-constrained in solar experiments and KamLAND, θ_{13} ($\neq 0$) by R-SBL experiments, θ_{23} by atmospheric experiments and $|\Delta m^2_{31,32}|$ by atmospheric and A-LBL experiments, the uncertainties arise mostly due to the value of δ_{CP}. Presently, the best fit of δ_{CP} hints at $3\pi/2$ for IO, indicating maximal CP violation in the lepton sector. The upcoming A-LBL experiments such as DUNE and T2HK shall explore the CPV phase. In these experiments, the CP asymmetry can be intrinsic due to presence of $\sin\delta_{CP}$ term and can also be due to matter effect experienced by neutrinos and antineutrinos while propagating through Earth matter. This fake CPV due to matter effect must be disentangled from the genuine CPV parameter δ_{CP}. Other possible new physics effects like sterile neutrinos [114–116], non-standard interactions [117–120], that can induce fake CPV must also be taken into consideration in the measurement of δ_{CP}.

1.5.1.3 Octant Degeneracy

The PMNS matrix is yet to be fully fixed as the octant of θ_{23} and the value of δ_{CP} are unknown. If the value of θ_{23} is measured to be $\pi/4$, it means the mass eigenstate ν_3 is comprised of an approximately equal amount of ν_μ and

ν_τ, indicating some *unknown* symmetry between the second and the third lepton generations. Whether θ_{23} is exactly equal to 45°, in the lower octant (LO, $\theta_{23} < 45°$), or in the higher octant (HO, $\theta_{23} > 45°$) is of interest to pursue. Particularly, $\theta_{23} = \pi/4$ is allowed in many neutrino mass models as a consequence of the exact $\mu - \tau$ symmetry [121]. The deviation of θ_{23} from $\pi/4$ will serve as useful model discriminator [122, 123] and requires a precision measurement in the upcoming atmospheric and A-LBL experiments.

1.5.2 Beyond standard 3ν neutrino oscillation

1.5.2.1 Sterile neutrinos

Whether there exists additional species of neutrinos is one of the fundamental questions in neutrino physics and cosmology. Such neutrinos cannot take part directly in weak interactions, but with the active neutrinos. Experimentally, accelerator anomalies from LSND [88] and MiniBooNE [124], and reactor antineutrino anomalies [125] are explained using sterile-active oscillations with the assumption of one or two sterile neutrinos. The mass-squared difference that could explain the LSND $\bar{\nu}_e$ excess in $\bar{\nu_\mu} \rightarrow \bar{\nu}_e$ oscillation measurement is $\Delta m^2 = 1eV^2$, suggesting the presence of a sterile neutrino [126]. Event rate deficit of ν_e candidate in solar experiments GALLEX and SAGE also favour the sterile neutrino hypothesis in the measurement of $\nu_e \rightarrow \nu_e$ disappearance [127, 128]. Also, long-lived sterile neutrinos at the keV scale might serve as a warm dark matter candidate [129].

1.5.2.2 Nature of neutrino: Dirac or Majorana

A lepton and its antiparticle possess opposite lepton numbers and are distinguishable. But if neutrino is a Majorana particle, it is its own antiparticle [130], leading to lepton number violation as a direct consequence. The tiny masses of three known neutrinos make it extremely difficult to identify their nature, *i.e.*, whether they are the Dirac or Majorana particles. At present

the only experimentally feasible way to probe the Majorana nature of massive neutrinos is to observe $0\nu\beta\beta$ decays of some even-even nuclei, given by the process $N(A,Z) \rightarrow N(A,Z{+}2){+}2e^{-}$, which occur via an exchange of the virtual Majorana neutrinos between two beta decays [131].

1.5.2.3 Absolute scale of neutrino mass

It is important to note that the phenomenon of neutrino oscillation can only probe the mass squared differences of the neutrinos but not their absolute masses. A determination of absolute mass scale is performed by a number of non-oscillation experiments. There are tritium beta decay experiments which measure the absolute mass of neutrinos. The effective electron antineutrino mass is measured in the beta decay ${}^{3}_{1}H \rightarrow {}^{3}_{2}H + e^{-} + \bar{\nu}_{e}$, given by

$$< m_{e} > \equiv \sqrt{\sum_{i=1}^{3} m_{i}^{2} |U_{ei}|^{2}} \tag{1.16}$$

The combined data of Troitsk [132] and Mainz [133] experiments give the upper bound of electron neutrino mass as < 1.8 eV. The combined result of first and second campaign of neutrino-mass measurement of KATRIN gives an improved upper limit of < 0.8 eV [134] for the mass of electron antineutrino. There are also weak bounds on muon neutrino [135] and tau neutrino [136] masses coming from pion and tau decay as < 0.17 MeV and < 18.2 MeV respectively. The neutrinoless double beta decay ($0\nu\beta\beta$) experiments which can probe Majorana nature of the neutrinos can also put constraint on the effective Majorana neutrino mass. The decay width of a particular Neutrinoless Double Beta Decay (NDBD) process mediated by light neutrino can be written as,

$$\Gamma^{0\nu} = 1/T^{0\nu}_{1/2} = G^{\nu}(Q,Z)|M^{0\nu\beta\beta}|^{2}\frac{|m_{\beta\beta}|^{2}}{m_{e}^{2}}$$

, where $G^{\nu}(Q,Z)$ is the phase factor, $M^{0\nu\beta\beta}$ is the nuclear matrix element (NME) and $m_{\beta\beta}$ is the effective Majorana mass. $T^{0\nu}_{1/2}$ represents the half-life of the decay of the isotope under consideration. The effective Majorana mass is $|\sum_{i=1}^{3} U_{ei}^{2} m_{i}|$,

where m_i are the Majorana masses of the three light neutrinos.

Experiments like CUORE, Gerda and KamLAND-Zen have set lower limits on the half-life of isotopes ^{130}Te ($T^{0\nu}_{1/2} > 3.2 \times 10^{25}$), ^{76}Ge ($T^{0\nu}_{1/2} > 9 \times 10^{25}$) and ^{136}Xe ($T^{0\nu}_{1/2} > 1.07 \times 10^{26}$), respectively. These bounds on the half-life from the above experiments give the upper limits on the effective mass of $m_{\beta\beta} < 75 - 350$ meV by CUORE [137], $m_{\beta\beta} < 104 - 228$ meV by Gerda [138] and $m_{\beta\beta} < 104 - 228$ meV by KamLAND-Zen [139], respectively where the bounds on the corresponding NMEs can be found in Ref [140]. An upper bound on the sum of active neutrino masses as 0.118 eV comes from cosmology [141]. From the neutrino oscillation experiments we know that the two mass squared differences which govern the oscillation of the three generations of neutrinos are of the order of 10^{-5} eV^2 and 10^{-3} eV^2. Thus, the oscillation data together with the cosmological bound signify that the neutrino masses are much smaller than the masses of the charged leptons.

1.5.2.4 CPT/Lorentz Violation

CPT violation are related to Lorentz symmetry breaking in local field theories [142]. CPT interchanges the $\nu_\alpha \to \nu_\beta$ and $\bar{\nu}_\beta \to \bar{\nu}_\alpha$ $(\alpha, \beta = e, \mu, \tau)$ oscillation channels. Hence, CPT violation can be explored by measuring the difference of these two channels, given by CPT asymmetry, $\mathcal{A}^{CPT} = P_{\nu_\alpha \to \nu_\beta} - P_{\bar{\nu}_\beta \to \bar{\nu}_\alpha}$. Ongoing accelerator neutrino experiments measure $\nu_\mu \to \nu_e$ and $\nu_\mu \to \nu_\mu$ oscillation channels and anti-neutrino counterparts. As there is no experiments presently that can measure the CPT asymmetry in appearance channels as the $\bar{\nu}_e \to \bar{\nu}_\mu$ is missing, CPT violation can be explored via the disappearance channels. For CPT violation to be observed, there has to be a finite difference between the set of oscillation parameters defining the neutrino and anti-neutrino oscillation probabilities, defined as $\delta_{\nu\bar{\nu}}(X) = X - \bar{X}$, where X are the six parameters in neutrino oscillation and $\bar{X}$ are the corresponding parameters describing anti-neutrino oscillation. An interesting work on CPT violation is recently published and can be found in Ref [143].

1.6 Scope of the Thesis

The work of this thesis involves the sensitivity of three terrestrial experiments: two A-LBL experiments (T2K-II and NOνA) and one R-MBL experiments JUNO to address the three outstanding problems in neutrino oscillation physics *viz.* determination of neutrino mass hierarchy, exploring leptonic CP violation and resolving the octant degeneracy of θ_{23}.

Chapter 2 forms the motivation of the thesis. We describe the three neutrino oscillation phenomenology in great details. We present a derivation of neutrino oscillation probabilities relevant to A-LBL experiments and discuss the significance of the relevant oscillation channels. We also revisit the parameter degeneracy in neutrino oscillation in context of the present global data fits. We describe the limitations of A-LBL experiments due to the degeneracies and emphasize on our framework.

In chapter 3, we give the description of the oscillation experiments which we have studied in the thesis. We describe the configurations of the above experiments and present the simulated event spectra of the selected appearance and disappearance channels.

Chapter 4 covers the results of our neutrino oscillation analysis. We discuss the sensitivities of T2K-II, NOνA and JUNO to mass hierarchy and CPV by taking their projected exposures. We also comment on the effect of varying T2K-II exposure on the above issues.

In chapter 5, we present our results on the precision measurements of the oscillation parameters θ_{13}, θ_{23}, Δm^2_{31} and δ_{CP}, and the combined sensitivity to resolving the octant degeneracy by the considered experiments.

Finally, we summarize the thesis and give the impact of our work.

Bibliography

[1] Ellis, C. D. & Wooster, W. A. The average energy of disintegration of radium E. *Proceedings of the Royal Society of London. Series A, Containing Papers of a Mathematical and Physical Character* **117** (776), 109–123, 1927.

[2] Dickinson, R. *et al.* Raman spectra of polyatomic gases. *Physical Review* **34** (4), 582, 1929.

[3] Heitler, W. & Herzberg, G. Gehorchen die stickstoffkerne der boseschen statistik? *Naturwissenschaften* **17** (34), 673–674, 1929.

[4] Pauli, W. Pauli letter collection: letter to lise meitner. Tech. Rep., 1930.

[5] Fermi, E. An attempt at a theory of 'beta'ray emission. *Ricerca Scientifica* **4** (2), 491–495, 1933.

[6] Chadwick, J. Possible existence of a neutron. *Nature* **129** (3252), 312–312, 1932.

[7] Fermi, E. Tentativo di una teoria dei raggi ß. *Ricerca Scient* **2**, 12, 1933.

[8] Cowan, C. *et al.* A test of neutrino-antineutrino identity. *Il Nuovo Cimento (1955-1965)* **3** (3), 649–651, 1956.

[9] Danby, G. *et al.* Observation of high-energy neutrino reactions and the existence of two kinds of neutrinos. *Physical Review Letters* **9** (1), 36, 1962.

[10] Kodama, K. *et al.* Observation of tau neutrino interactions. *Physics Letters B* **504** (3), 218–224, 2001.

[11] Weinberg, S. A Model of Leptons. *Phys. Rev. Lett.* **19**, 1264–1266, 1967.

[12] Zyla, P. *et al.* Particle Data Group. *Prog. Theor. Exp. Phys.* **083C01**, 2020.

[13] Schael, S. *et al.* Precision electroweak measurements on the Z resonance. *Phys. Rept.* **427**, 257–454, 2006. hep-ex/0509008.

[14] Lee, T. D. & Yang, C.-N. Question of Parity Conservation in Weak Interactions. *Phys. Rev.* **104**, 254–258, 1956.

[15] Wu, C. S. *et al.* Experimental Test of Parity Conservation in β Decay. *Phys. Rev.* **105**, 1413–1414, 1957.

[16] Goldhaber, M. *et al.* Helicity of Neutrinos. *Phys. Rev.* **109**, 1015–1017, 1958.

[17] Maki, Z. *et al.* Remarks on the unified model of elementary particles. *Progress of Theoretical Physics* **28** (5), 870–880, 1962.

[18] Pontecorvo, B. Neutrino experiments and the problem of conservation of leptonic charge. *Sov. Phys. JETP* **26** (984-988), 165, 1968.

[19] Nakamura, K. & Petcov, S. Neutrino mass, mixing, and oscillations. *K. Nakamura et al.(Particle Data Group), J. Phys. G* **37**, 075021, 2010.

[20] Diwan, M. V. *et al.* Long-Baseline Neutrino Experiments. *Ann. Rev. Nucl. Part. Sci.* **66**, 47–71, 2016. 1608.06237.

[21] Giunti, C. & Kim, C. W. *Fundamentals of Neutrino Physics and Astrophysics*, 2007.

[22] Davis, R., Jr. *et al.* Search for neutrinos from the sun. *Phys. Rev. Lett.* **20**, 1205–1209, 1968.

[23] Pontecorvo, B. Inverse beta process. *Camb. Monogr. Part. Phys. Nucl. Phys. Cosmol.* **1**, 25–31, 1991.

[24] Alvarez, L. W. A Proposed Experimental Test of the Neutrino Theory , 1949.

[25] Bahcall, J. N. *et al.* Solar models: Current epoch and time dependences, neutrinos, and helioseismological properties. *Astrophys. J.* **555**, 990–1012, 2001. astro-ph/0010346.

[26] Anselmann, P. *et al.* Implications of the GALLEX determination of the solar neutrino flux. *Physics Letters B* **285** (4), 390–397, 1992.

[27] Anselmann, P. *et al.* Solar neutrinos observed by GALLEX at Gran Sasso. *Physics Letters B* **285** (4), 376–389, 1992.

[28] Anselmann, P. *et al.* GALLEX solar neutrino observations. The results from GALLEX I and early results from GALLEX II. *Physics Letters B* **314** (3-4), 445–458, 1993.

[29] Anselmann, P. *et al.* GALLEX results from the first 30 solar neutrino runs. *Phys. Lett. B* **327**, 377–385, 1994.

[30] Anselmann, P. *et al.* GALLEX solar neutrino observations: Complete results for GALLEX II. *Phys. Lett. B* **357**, 237–247, 1995. [Erratum: Phys.Lett.B 361, 235–236 (1995)].

[31] Altmann, M. *et al.* GNO solar neutrino observations: Results for GNO I. *Phys. Lett. B* **490**, 16–26, 2000. hep-ex/0006034.

[32] Altmann, M. *et al.* Complete results for five years of GNO solar neutrino observations. *Physics Letters B* **616** (3-4), 174–190, 2005.

[33] Abazov, A. I. *et al.* Search for neutrinos from sun using the reaction $^{71}Ga(\nu_e, e^-)^{71}Ge$. *Phys. Rev. Lett.* **67**, 3332–3335, 1991.

[34] Abdurashitov, J. N. *et al.* Results from SAGE. *Phys. Lett. B* **328**, 234–248, 1994.

[35] Abdurashitov, J. N. *et al.* Measurement of the solar neutrino capture rate by SAGE and implications for neutrino oscillations in vacuum. *Phys. Rev. Lett.* **83**, 4686–4689, 1999. astro-ph/9907131.

[36] Abdurashitov, J. N. *et al.* Measurement of the solar neutrino capture rate with gallium metal. *Phys. Rev. C* **60**, 055801, 1999. astro-ph/9907113.

[37] Abdurashitov, J. N. *et al.* Solar neutrino flux measurements by the Soviet-American Gallium Experiment (SAGE) for half the 22 year solar cycle. *J. Exp. Theor. Phys.* **95**, 181–193, 2002. astro-ph/0204245.

[38] Kuzmin, V. Zhetf, 49 (1965), 1532; kuz'min va. *Sov. Phys. JETP* **22**, 1051, 1966.

[39] Koshiba, M. Observational neutrino astrophysics. *Phys. Rept.* **220**, 229–381, 1992.

[40] Fukuda, Y. *et al.* Solar neutrino data covering solar cycle 22. *Phys. Rev. Lett.* **77**, 1683–1686, 1996.

[41] Hosaka, J. *et al.* Solar neutrino measurements in Super-Kamiokande-I. *Phys. Rev. D* **73**, 112001, 2006. hep-ex/0508053.

[42] Boger, J. *et al.* The Sudbury neutrino observatory. *Nucl. Instrum. Meth. A* **449**, 172–207, 2000. nucl-ex/9910016.

[43] Ahmad, Q. R. *et al.* Measurement of the rate of $\nu_e + d \rightarrow p + p + e^-$ interactions produced by ^{8}B solar neutrinos at the Sudbury Neutrino Observatory. *Phys. Rev. Lett.* **87**, 071301, 2001. nucl-ex/0106015.

[44] Ahmad, Q. R. *et al.* Direct evidence for neutrino flavor transformation from neutral current interactions in the Sudbury Neutrino Observatory. *Phys. Rev. Lett.* **89**, 011301, 2002. nucl-ex/0204008.

[45] Achar, C. V. *et al.* Detection of muons produced by cosmic ray neutrinos deep underground. *Phys. Lett.* **18**, 196–199, 1965.

[46] Reines, F. *et al.* Evidence for high-energy cosmic ray neutrino interactions. *Phys. Rev. Lett.* **15**, 429–433, 1965.

[47] Hirata, K. S. *et al.* Experimental Study of the Atmospheric Neutrino Flux. *Phys. Lett. B* **205**, 416, 1988.

[48] Casper, D. *et al.* Measurement of atmospheric neutrino composition with IMB-3 detector. *Phys. Rev. Lett.* **66**, 2561–2564, 1991.

[49] Becker-Szendy, R. *et al.* Electron- and muon-neutrino content of the atmospheric flux. *Phys. Rev. D* **46**, 3720–3724, 1992.

[50] Goodman, M. C. The Atmospheric neutrino anomaly in Soudan-2. *Nucl. Phys. B Proc. Suppl.* **38**, 337–342, 1995.

[51] Fukuda, Y. *et al.* Evidence for oscillation of atmospheric neutrinos. *Phys. Rev. Lett.* **81**, 1562–1567, 1998. hep-ex/9807003.

[52] Hulth, P. O. Ultra high energy neutrino telescopes. *Int. J. Mod. Phys. A* **21**, 1914–1924, 2006.

[53] Hirata, K. *et al.* Observation in the Kamiokande-II detector of the neutrino burst from supernova SN1987A. *Physical Review D* **38** (2), 448, 1988.

[54] Alexeyev, E. *et al.* Detection of the neutrino signal from SN 1987A in the LMC using the INR Baksan underground scintillation telescope. *Physics Letters B* **205** (2-3), 209–214, 1988.

[55] Nellen, L. *et al.* Neutrino production through hadronic cascades in AGN accretion disks. *Physical Review D* **47** (12), 5270, 1993.

[56] Waxman, E. & Bahcall, J. N. High-energy neutrinos from cosmological gamma-ray burst fireballs. *Phys. Rev. Lett.* **78**, 2292–2295, 1997. astro-ph/9701231.

[57] Vogel, P. *et al.* Neutrino oscillation studies with reactors. *Nature Communications* **6** (1), 1–12, 2015.

[58] Kwon, H. *et al.* Search for Neutrino Oscillations at a Fission Reactor. *Phys. Rev. D* **24**, 1097–1111, 1981.

[59] Zacek, G. *et al.* Neutrino Oscillation Experiments at the Gosgen Nuclear Power Reactor. *Phys. Rev. D* **34**, 2621–2636, 1986.

[60] Afonin, A. I. *et al.* $\bar{\nu}_e$ Spectra at Two Distances From the Reactor of the Rovno Nuclear Power Plant: Search for Oscillations. *JETP Lett.* **45**, 247–251, 1987.

[61] Vidyakin, G. S. *et al.* Limitations on the characteristics of neutrino oscillations. *JETP Lett.* **59**, 390–393, 1994.

[62] Declais, Y. *et al.* Search for neutrino oscillations at 15-meters, 40-meters, and 95-meters from a nuclear power reactor at Bugey. *Nucl. Phys. B* **434**, 503–534, 1995.

[63] Greenwood, Z. D. *et al.* Results of a two position reactor neutrino oscillation experiment. *Phys. Rev. D* **53**, 6054–6064, 1996.

[64] Apollonio, M. *et al.* Initial results from the CHOOZ long baseline reactor neutrino oscillation experiment. *Phys. Lett. B* **420**, 397–404, 1998. hep-ex/9711002.

[65] Apollonio, M. *et al.* Limits on neutrino oscillations from the CHOOZ experiment. *Phys. Lett. B* **466**, 415–430, 1999. hep-ex/9907037.

[66] Apollonio, M. *et al.* Search for neutrino oscillations on a long base-line at the CHOOZ nuclear power station. *The European Physical Journal C-Particles and Fields* **27** (3), 331–374, 2003.

[67] Boehm, F. *et al.* Results from the Palo Verde neutrino oscillation experiment. *Phys. Rev. D* **62**, 072002, 2000. hep-ex/0003022.

[68] Boehm, F. *et al.* Search for neutrino oscillations at the Palo Verde nuclear reactors. *Phys. Rev. Lett.* **84**, 3764–3767, 2000. hep-ex/9912050.

[69] Boehm, F. *et al.* Final results from the Palo Verde neutrino oscillation experiment. *Physical Review D* **64** (11), 112001, 2001.

[70] An, F. *et al.* Observation of electron-antineutrino disappearance at Daya Bay. *Physical Review Letters* **108** (17), 171803, 2012.

[71] An, F. P. *et al.* Spectral measurement of electron antineutrino oscillation amplitude and frequency at Daya Bay. *Phys. Rev. Lett.* **112**, 061801, 2014. 1310.6732.

[72] Ahn, J. K. *et al.* Observation of Reactor Electron Antineutrino Disappearance in the RENO Experiment. *Phys. Rev. Lett.* **108**, 191802, 2012. 1204.0626.

[73] Abe, Y. *et al.* Indication of Reactor $\bar{\nu}_e$ Disappearance in the Double Chooz Experiment. *Phys. Rev. Lett.* **108**, 131801, 2012. 1112.6353.

[74] Abe, Y. *et al.* Background-independent measurement of θ_{13} in Double Chooz. *Phys. Lett. B* **735**, 51–56, 2014. 1401.5981.

[75] Esteban, I. *et al.* The fate of hints: updated global analysis of three-flavor neutrino oscillations. *JHEP* **09**, 178, 2020. 2007.14792.

[76] de Salas, P. F. *et al.* 2020 global reassessment of the neutrino oscillation picture. *JHEP* **02**, 071, 2021. 2006.11237.

[77] Eguchi, K. *et al.* First results from KamLAND: Evidence for reactor anti-neutrino disappearance. *Phys. Rev. Lett.* **90**, 021802, 2003. hep-ex/0212021.

[78] Araki, T. *et al.* Measurement of neutrino oscillation with KamLAND: Evidence of spectral distortion. *Phys. Rev. Lett.* **94**, 081801, 2005. hep-ex/0406035.

[79] Adamson, P. *et al.* The NuMI Neutrino Beam. *Nucl. Instrum. Meth. A* **806**, 279–306, 2016. 1507.06690.

[80] Diwan, M. V. Status of the MINOS experiment. *eConf* **C0209101**, TH08, 2002. hep-ex/0211026.

[81] Tzanankos, G. *et al.* MINOS+: a Proposal to FNAL to run MINOS with the medium energy NuMI beam , 2011.

[82] Ayres, D. S. *et al.* NOvA: Proposal to Build a 30 Kiloton Off-Axis Detector to Study $\nu_\mu \rightarrow \nu_e$ Oscillations in the NuMI Beamline , 2004. hep-ex/0503053.

[83] Nayak, N. *A Joint Measurement of ν_μ-Disappearance and ν_e-Appearance in the NuMI Beam Using the NOvA Experiment.* Ph.D. thesis, University of California, Irvine, 2021.

[84] Bergsma, F. *et al.* A Search for Neutrino Oscillations. *Z. Phys. C* **40**, 171, 1988.

[85] Dydak, F. *et al.* A search for ν_μ oscillations in the Δm^2 range 0.3-90 eV^2. *Phys. Lett. B* **134** (281), 90688–9, 1984.

[86] Stockdale, I. E. *et al.* Search for ν_μ and $\bar{\nu}$ Oscillations in the Mass Range $15 - \mathrm{eV}^2/c^4 < \delta M^2 < 1000 - \mathrm{eV}^2/c^4$. *Conf. Proc. C* **841031**, 258, 1984.

[87] Angelini, C. *et al.* New Experimental Limits on $\nu_\mu \rightarrow \nu_e$ Oscillations. *Phys. Lett., B* **179** (3), 307–312, 1986.

[88] Aguilar-Arevalo, A. *et al.* Evidence for neutrino oscillations from the observation of $\bar{\nu}_e$ appearance in a $\bar{\nu}_\mu$ beam. *Phys. Rev. D* **64**, 112007, 2001. hep-ex/0104049.

[89] Astier, P. *et al.* Search for $\nu_\mu \to \nu_e$ oscillations in the NOMAD experiment. *Phys. Lett. B* **570**, 19–31, 2003. hep-ex/0306037.

[90] Armbruster, B. *et al.* Upper limits for neutrino oscillations $\nu_\mu \to \nu_e$ from muon decay at rest. *Physical Review D* **65** (11), 112001, 2002.

[91] Eskut, E. *et al.* New results from a search for $\nu_\mu \to \nu_\tau$ and $\nu_e \to \nu_\tau$ oscillation. *Phys. Lett. B* **497**, 8–22, 2001.

[92] Aguilar-Arevalo, A. *et al.* Evidence for neutrino oscillations from the observation of $\bar{\nu}_e$ appearance in a $\bar{\nu}_\mu$ beam. *Phys. Rev. D* **64**, 112007, 2001. hep-ex/0104049.

[93] Athanassopoulos, C. *et al.* Evidence for $\nu_\mu \to \nu_e$ neutrino oscillations from LSND. *Phys. Rev. Lett.* **81**, 1774–1777, 1998. nucl-ex/9709006.

[94] Ahn, M. H. *et al.* Indications of neutrino oscillation in a 250 km long baseline experiment. *Phys. Rev. Lett.* **90**, 041801, 2003. hep-ex/0212007.

[95] Ahn, M. H. *et al.* Search for electron neutrino appearance in a 250 km long baseline experiment. *Phys. Rev. Lett.* **93**, 051801, 2004. hep-ex/0402017.

[96] Ahn, S. H. *et al.* Detection of accelerator produced neutrinos at a distance of 250 km. *Phys. Lett. B* **511**, 178–184, 2001. hep-ex/0103001.

[97] Yamamoto, S. *et al.* Improved Search for $\nu_\mu \to \nu_e$ Oscillation in a Long-Baseline Accelerator Experiment. *Physical Review Letters* **96** (18), 181801, 2006.

[98] Komatsu, M. *et al.* Sensitivity to θ_{13} of the CERN to Gran Sasso neutrino beam. *Journal of Physics G: Nuclear and Particle Physics* **29** (2), 443, 2003.

[99] Arneodo, F. *et al.* The ICARUS experiment: A Second generation proton decay experiment and neutrino observatory at the Gran Sasso Laboratory , 2001. hep-ex/0103008.

[100] Itow, Y. *et al.* The JHF-Kamioka neutrino project. In *3rd Workshop on Neutrino Oscillations and Their Origin (NOON 2001)*. 239–248, 2001. hep-ex/0106019.

[101] Ayres, D. *et al.* Letter of Intent to build an Off-axis Detector to study numu to nue oscillations with the NuMI Neutrino Beam , 2002. hep-ex/0210005.

[102] Nath, A. & Francis, N. K. Detection techniques and investigation of different neutrino experiments. *Int. J. Mod. Phys. A* **36** (13), 2130008, 2021. 1804.08467.

[103] Formaggio, J. A. & Zeller, G. P. From eV to EeV: Neutrino Cross Sections Across Energy Scales. *Rev. Mod. Phys.* **84**, 1307–1341, 2012. 1305.7513.

[104] Esteban, I. *et al.* Global analysis of three-flavour neutrino oscillations: synergies and tensions in the determination of θ_{23}, δ_{CP}, and the mass ordering. *JHEP* **01**, 106, 2019. 1811.05487.

[105] de Salas, P. *et al.* Status of neutrino oscillations 2017. *arXiv:1708.01186* , 2017.

[106] Bernabeu, J. *et al.* Atmospheric neutrino oscillations, θ_{13} and neutrino mass hierarchy. *Nucl. Phys. B* **669**, 255–276, 2003. hep-ph/0305152.

[107] Dighe, A. S. & Smirnov, A. Y. Identifying the neutrino mass spectrum from the neutrino burst from a supernova. *Phys. Rev. D* **62**, 033007, 2000. hep-ph/9907423.

[108] Petcov, S. T. & Piai, M. The LMA MSW solution of the solar neutrino problem, inverted neutrino mass hierarchy and reactor neutrino experiments. *Phys. Lett. B* **533**, 94–106, 2002. hep-ph/0112074.

[109] Fukugita, M. & Yanagida, T. Baryogenesis Without Grand Unification. *Phys. Lett. B* **174**, 45–47, 1986.

[110] Buchmuller, W. *et al.* Leptogenesis for pedestrians. *Annals Phys.* **315**, 305–351, 2005. hep-ph/0401240.

[111] Davidson, S. *et al.* Leptogenesis. *Phys. Rept.* **466**, 105–177, 2008. 0802.2962.

[112] Bilenky, S. M. & Giunti, C. Neutrinoless double-beta decay: A brief review. *Mod. Phys. Lett. A* **27**, 1230015, 2012. 1203.5250.

[113] Christenson, J. H. *et al.* Evidence for the 2π Decay of the K_2^0 Meson. *Phys. Rev. Lett.* **13**, 138–140, 1964.

[114] Gandhi, R. *et al.* The impact of sterile neutrinos on CP measurements at long baselines. *JHEP* **11**, 039, 2015. 1508.06275.

[115] Dutta, D. *et al.* Capabilities of long-baseline experiments in the presence of a sterile neutrino. *JHEP* **11**, 122, 2016. 1607.02152.

[116] Berryman, J. M. *et al.* Sterile neutrino at the deep underground neutrino experiment. *Physical Review D* **92** (7), 073012, 2015.

[117] Esteban, I. *et al.* Updated constraints on non-standard interactions from global analysis of oscillation data. *Journal of High Energy Physics* **2018** (8), 1–33, 2018.

[118] Grossman, Y. Non-standard neutrino interactions and neutrino oscillation experiments. *Physics Letters B* **359** (1-2), 141–147, 1995.

[119] Masud, M. *et al.* Probing the CP violation signal at DUNE in the presence of non-standard neutrino interactions. *Journal of Physics G: Nuclear and Particle Physics* **43** (9), 095005, 2016.

[120] Coloma, P. Non-standard interactions in propagation at the Deep Underground Neutrino Experiment. *Journal of High Energy Physics* **2016** (3), 1–27, 2016.

[121] Xing, Z.-z. & Zhou, S. A partial $\mu - \tau$ symmetry and its prediction for leptonic CP violation. *Phys. Lett. B* **737**, 196–200, 2014. 1404.7021.

[122] Luo, S. & Xing, Z.-z. Resolving the octant of θ_{23} via radiative $\mu-\tau$ symmetry breaking. *Phys. Rev. D* **90** (7), 073005, 2014. 1408.5005.

[123] Zhou, Y.-L. μ-τ reflection symmetry and radiative corrections , 2014. 1409.8600.

[124] Aguilar-Arevalo, A. A. *et al.* Event Excess in the MiniBooNE Search for $\bar{\nu}_\mu \to \bar{\nu}_e$ Oscillations. *Phys. Rev. Lett.* **105**, 181801, 2010. 1007.1150.

[125] Mention, G. *et al.* The Reactor Antineutrino Anomaly. *Phys. Rev. D* **83**, 073006, 2011. 1101.2755.

[126] Gariazzo, S. *et al.* Updated global 3+ 1 analysis of short-baseline neutrino oscillations. *Journal of High Energy Physics* **2017** (6), 1–38, 2017.

[127] Acero, M. A. *et al.* Limits on ν_e and $\bar{\nu}_e$ disappearance from Gallium and reactor experiments. *Physical Review D* **78** (7), 073009, 2008.

[128] Giunti, C. & Laveder, M. Statistical Significance of the Gallium Anomaly. *Physical Review C* **83** (6), 065504, 2011.

[129] Bode, P. *et al.* Halo formation in warm dark matter models. *Astrophys. J.* **556**, 93–107, 2001. astro-ph/0010389.

[130] Majorana, E. Teoria simmetrica dell'elettrone e del positrone. *Nuovo Cim.* **14**, 171–184, 1937.

[131] Furry, W. H. On transition probabilities in double beta-disintegration. *Phys. Rev.* **56**, 1184–1193, 1939.

[132] Aseev, V. N. *et al.* An upper limit on electron antineutrino mass from Troitsk experiment. *Phys. Rev. D* **84**, 112003, 2011. 1108.5034.

[133] Kraus, C. *et al.* Final results from phase II of the Mainz neutrino mass search in tritium β decay. *The European Physical Journal C-Particles and Fields* **40** (4), 447–468, 2005.

[134] Aker, M. *et al.* Direct neutrino-mass measurement with sub-electronvolt sensitivity. *Nature Phys.* **18** (2), 160–166, 2022. 2105.08533.

[135] Assamagan, K. *et al.* Upper limit of the muon-neutrino mass and charged pion mass from momentum analysis of a surface muon beam. *Phys. Rev. D* **53**, 6065–6077, 1996.

[136] Barate, R. *et al.* An Upper limit on the tau-neutrino mass from three-prong and five-prong tau decays. *Eur. Phys. J. C* **2**, 395–406, 1998.

[137] Adams, D. Q. *et al.* Improved Limit on Neutrinoless Double-Beta Decay in ^{130}Te with CUORE. *Phys. Rev. Lett.* **124** (12), 122501, 2020. 1912.10966.

[138] Agostini, M. *et al.* Probing Majorana neutrinos with double-β decay. *Science* **365**, 1445, 2019. 1909.02726.

[139] Gando, A. *et al.* Search for Majorana Neutrinos near the Inverted Mass Hierarchy Region with KamLAND-Zen. *Phys. Rev. Lett.* **117** (8), 082503, 2016. [Addendum: Phys.Rev.Lett. 117, 109903 (2016)], 1605.02889.

[140] Vergados, J. D. *et al.* Neutrinoless double beta decay and neutrino mass. *Int. J. Mod. Phys. E* **25** (11), 1630007, 2016. 1612.02924.

[141] Roy Choudhury, S. & Choubey, S. Updated Bounds on Sum of Neutrino Masses in Various Cosmological Scenarios. *JCAP* **09**, 017, 2018. 1806.10832.

[142] Greenberg, O. W. CPT Violation Implies Violation of Lorentz Invariance. *Physical Review Letters* **89** (23), 231602, 2002.

[143] Ngoc, T. V. *et al.* Stringent constraint on CPT violation with the synergy of T2K-II, NOνA extension, and JUNO. *Phys. Rev. D* **107** (1), 016013, 2023. 2210.13044.